JOURNAL OF MATERIALS SCIENCE 27 (1992) 6519–6524

Structural studies of phase transformations in ultrafine zirconia powders

E. BERNSTEIN, M. G. BLANCHIN, R. RAVELLE-CHAPUIS
Département de Physique des Matériaux, Université Claude Bernard Lyon I, 43 Bd. du 11 Novembre 1918, 69622 Villeurbanne Cédex, France

J. RODRIGUEZ-CARVAJAL
Institute Laue-Langevin, B.P. 156, 38042 Grenoble Cédex 9, France

The factors governing the existence of metastable cubic and tetragonal phases in zirconia powders are still controversial. In order to elucidate this question, the effects of calcination temperature on ultrafine powders prepared from different precursors by different low-temperature chemical routes were studied. The morphological and structural characteristics of the powders depending on the calcination temperature were determined by means of conventional and high-resolution transmission electron microscopy (CTEM and HREM) and X-ray diffraction methods (whole and peak profile fitting procedures). Important structural differences between the powders depending on the precursor were revealed by HREM. The presence of impurities and/or microstrains seems to play a major role in the stabilization of the cubic and the tetragonal phases.

1. Introduction

Low-temperature chemical reactions, like thermal decomposition of hydrous zirconia, have been widely used to obtain fine, sinteractive ZrO_2 powders. The factors governing the occurrence of the metastable tetragonal and cubic phases in ZrO_2 at room temperature, as a result of calcination of amorphous precursors, is still controversial. Various explanations such as effects due to crystallite size, strain or lattice defects, the role of impurities, structural similarities between the amorphous precursors and the metastable phases were reported by many authors, as recently reviewed [1].

The aim of the present work was to investigate this question further, by means of high-resolution techniques, to reveal the structural features accommodating phase transformations in zirconia powders obtained from different precursors, as a function of calcination temperature. Powders prepared by two different low-temperature chemical routes were studied by X-ray diffraction methods and transmission electron microscopy.

2. Experimental procedure

2.1. Powder preparation

Two amorphous hydrated zirconia powders, prepared at room temperature by different chemical routes were used as starting materials.

1. A powder, Z_1, obtained from a reaction of a solid zirconium basic sulphate (corresponding to the molar ratio $ZrO_2/SO_3 = 1.5$ mol) with a dilute solution of sodium hydroxide to extract the sulphate ions.

2. A powder, Z_2, prepared by precipitation of ZrO_2 hydroxide from a solution of oxychloride by addition of ammonia.

Both materials were subjected to the same thermal treatments, i.e. calcination for 1 h at temperatures ranging from 400–1000 °C. The products obtained at different temperatures, T in that range are labelled Z_1 (T) and Z_2 (T), respectively.

2.2. Characterization techniques

The specific surface area of the powders was measured by the multipoint BET method and the equivalent diameter of the particles was calculated from the equation $D = 6/\rho S$, where D is the particle diameter, ρ is the density assumed to be 5.8 g cm^{-3} [2] and S is the specific surface area.

The morphological features, size distribution and aggregation state of the powder particles were examined by conventional transmission electron microscopy (CTEM) in bright- and dark-field imaging modes. Observations were carried out in a Philips EM300 microscope operating at 100 kV. Electron diffraction was used to identify the crystalline phase of the particles. The TEM samples were prepared by direct deposition of the powders on to a carbon film mounted on copper grids.

In the case of very small particles, their size, morphology and structure were studied by high-resolution transmission electron microscopy (HREM). In this case the observations were carried out in a Jeol 200 CX-UHP2S microscope, operating at 200 kV, with a

0022–2461

point-to-point resolution of 0.22 nm. Optical diffractograms were obtained from these micrographs by forming the Fraunhofer diffraction pattern of the HREM images, using laser illumination on an optical bench [3], to identify the phase of individual crystallites.

X-ray powder diffraction (XRD) spectra of the samples were obtained with a Siemens D-500 diffractrometer using CuK_α radiation. Owing to severe overlapping of the 1 1 $\bar{1}$ and 1 1 1 peaks of monoclinic ZrO_2 with the 1 1 1 peak of tetragonal ZrO_2, a reliable determination of the phase concentration as well as of the crystallite size could only be achieved by using a pattern-fitting procedure. The structural refinement and quantitative determination of the proportion of phases were obtained by the Rietveld whole pattern-fitting method [4].

Crystallite sizes, d, and microstrains, ε, were calculated from the X-ray diffraction line broadening using a simplified method. This method is based on the size-strain separation through determination of the integral breadth, β, and of the full width at half maximum ($2w$) of the peaks considered, after correction for instrumental and $K_{\alpha 1-\alpha 2}$ doublet broadening. Following the single peak analysis by de Keijser *et al.* [5]

$$d = \lambda/\beta_c \cos\theta \quad (1)$$

and

$$\varepsilon = \beta_g/4 \operatorname{tg}\theta \quad (2)$$

where β_c and β_g are the constituent Cauchy and Gauss components of the peak profile assumed to be a Voigt function (i.e. a convolution of a Cauchy with a Gauss function) [6]. β_c and β_g were derived from the shape factor $2w/\beta$ using a rational approximation proposed by de Keijser *et al.* [5], β and $2w$ being obtained by a peak profile refinement procedure of pattern decomposition. Peaks were fitted in a reduced angular domain (typically from 21°–38°) assuming pseudo Voigt profile functions [7]. The size obtained from Equation 1 is called the effective crystallite size. In cases where the separation between size and strain contributions was not possible, the apparent crystallite size was obtained from the integral breath, β, as $d' = \lambda/\beta \cos\theta$.

The computer programs used for the Rietveld analysis and the peak profile refinement method were those of the Strap package [8].

3. Results

3.1. Size distribution

The variation of the specific surface area, as determined by BET, depending on the calcination temperature, together with the corresponding equivalent diameters of particles are given in Table I. A large decrease of the specific surface area at increasing calcination temperature is observed for both series Z_1 and Z_2.

The observations by CTEM at low magnification showed that the powders were formed by agglomerates with sizes ranging from 0.5–1.2 μm. The shape and size of these agglomerates do not seem to vary very much with calcination temperature [9]. Nevertheless, observations at higher magnification clearly revealed changes in particle size and morphology.

TABLE I Specific surface area, S, and equivalent diameter, D, as a function of the calcination temperature, T

T(°C)	S($m^2 g^{-1}$)		D(nm)	
	Z_1	Z_2	Z_1	Z_2
400	112	75	9	14
500	63	65	16	16
600	25		41	
700	14		74	
800	7.7		134	
850		12		86
900	6.3		164	
1000	5.4	4	192	257

3.2. TEM structural studies

3.2.1. Powders prepared from Z_1

As shown in Fig. 1a, CTEM micrographs could not reveal the morphology of the ultrafine particles forming the powder Z_1 (400). Diffraction patterns from this sample were formed by very weak rings which could correspond either to a cubic or to a tetragonal structure. Discrimination between the two structures was not possible by this technique due to the very small difference in the lattice parameters. High-magnification HREM images from this sample (Fig. 1b) showed that the particles are formed by randomly oriented small rounded crystallites, with a narrow size distribution (3–6 nm). Very few non-crystalline regions were observed. Optical diffractograms obtained from the HREM images of some individual grains could be indexed either on the basis of a cubic or of a tetragonal unit cell.

The main effect of increasing the calcination temperature up to 600 °C appeared to be a steady increase in the crystallite size d (8 nm $< d <$ 12 nm for Z_1 (500) and 12 nm $< d <$ 19 nm for Z_1 (600)), as shown in Fig. 2a. At 600 °C, the diffraction patterns exhibited also a few reflections corresponding to the monoclinic structure (Fig. 2b).

At $T > 700$ °C, the development of internal sintering was evident and it became more important as the temperature increased. This effect is indicated by arrows in Fig. 3a corresponding to Z_1 (800). The image contrast then became complex due to variations in crystal thickness, tangling of grain boundaries and superposition of particles with different orientations so that the determination of crystallite size from TEM observations became extremely difficult. Nevertheless HREM images from these samples revealed that the particles developed facets.

In the sample Z_1 (700), the diffraction patterns were consistent with coexisting tetragonal and monoclinic phases. In the samples calcined at higher temperatures, Z_1 (800) (Fig. 3b) and Z_1 (900), diffraction showed that the structure was mainly monoclinic, without any preferential orientation of the crystallites.

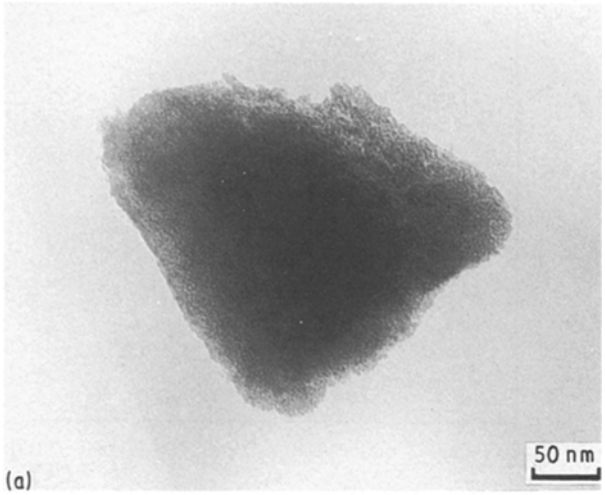

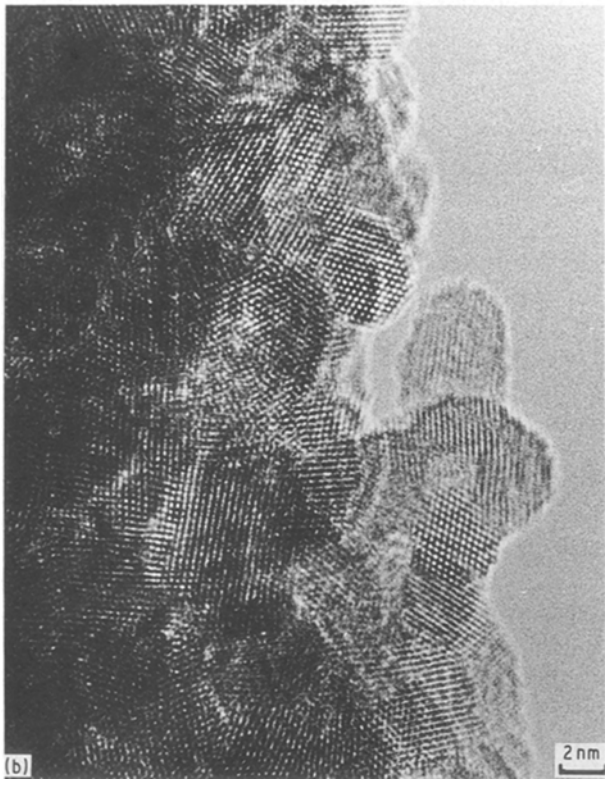

Figure 1 Sample Z_1 (400): (a) CTEM image, (b) HREM image.

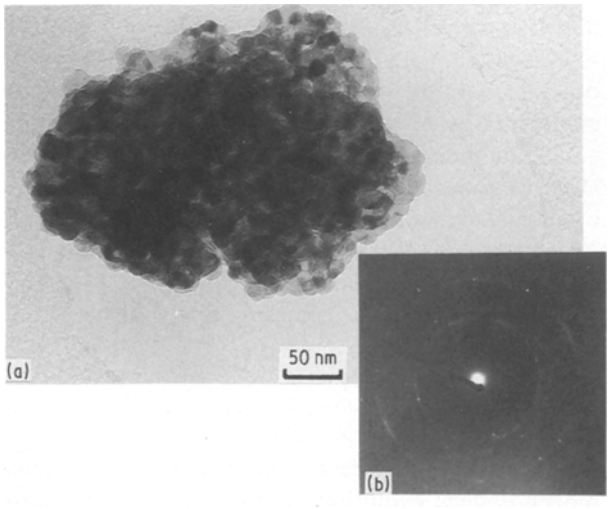

Figure 2 Sample Z_1 (600): (a) CTEM image, (b) electron diffraction pattern.

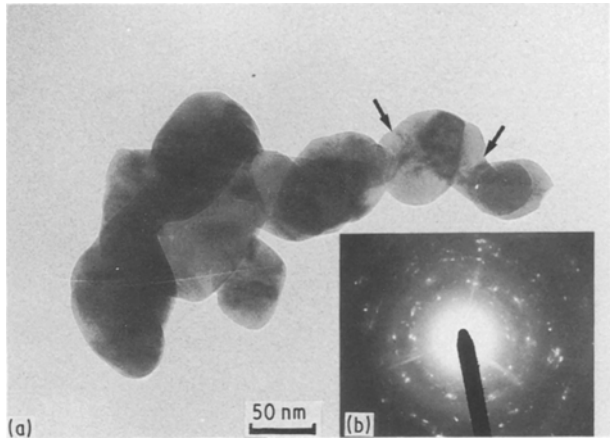

Figure 3 Sample Z_1 (800): (a) CTEM image, (b) electron diffraction pattern.

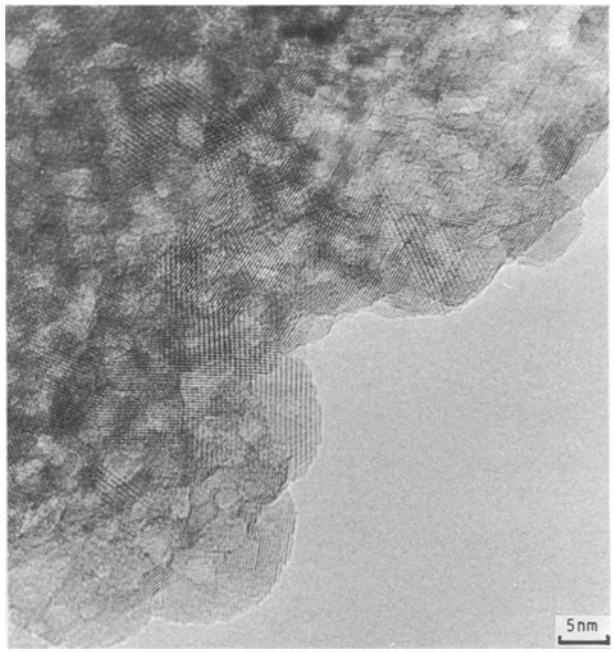

Figure 4 Sample Z_2 (500): HREM image.

3.2.2. Powders prepared from Z_2

TEM observations of powders obtained from the Z_2 precursor showed a rather similar dependence of crystallite size and morphology on calcination temperature, with respect to the previous series of samples. Nevertheless, some important differences were apparent.

HREM images of the sample Z_2 (500) (Fig. 4, for example), indicated that this powder is formed of crystallites with a relatively large size distribution (between 8 and 17 nm); these crystallites exhibited a large density of "etch pit-like" figures.

Sample Z_2 (850) (Fig. 5a) appeared to be rather similar to the powders calcined at lower temperatures (600 and 700 °C) from the Z_1 precursor. The main difference was the presence of the same kind of figures observed in Z_2 (500). The diffraction patterns from Z_2 (850) (Fig. 5b) corresponded mainly to a tetragonal structure. HREM observations of this sample revealed that it was formed by crystallites with sizes ranging

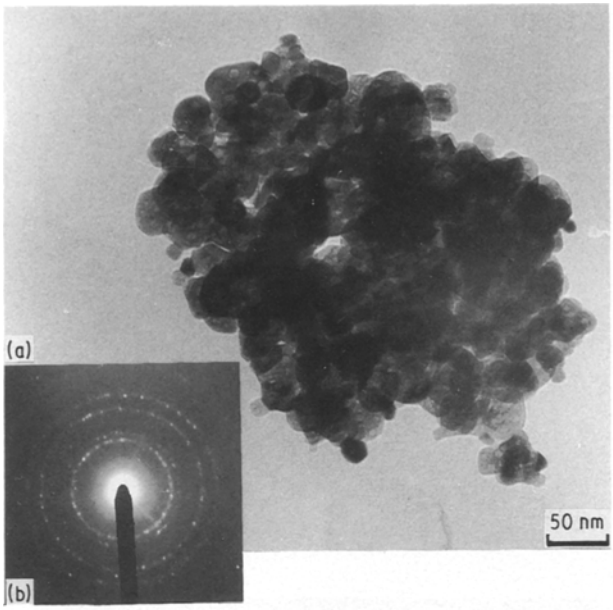

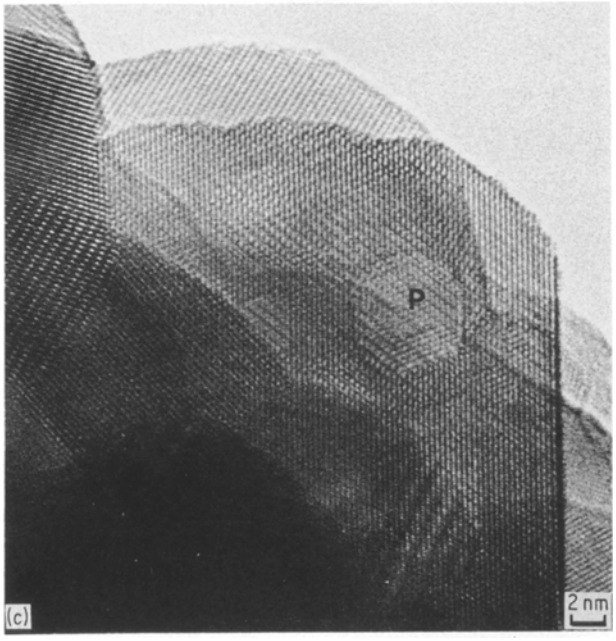

Figure 5 Sample Z_2 (850): (a) CTEM image, (b) electron diffraction pattern, (c) HREM image.

from 12–17 nm and that some particles developed facetting. Fig. 5c reproduces a high-magnification HREM image of a particle exhibiting what we have called "etch pit-like" figures (marked p in the figure). It can be seen on this figure that the "etch pit" regions give rise to the same HREM lattice image as the other crystal region, but with a lower intensity background. This indicates that they are neither amorphous inclusions, nor precipitates of other phases. The contrast features suggest that they are, in fact, superficial open pores. The density of these pores was lower in Z_2 (850) than in Z_2 (500), and nearly nil in Z_2 (1000).

3.3. XRD studies

Fig. 6 shows the relative proportion, as a function of calcination temperature, of the crystalline phases present in the samples. These values have been obtained

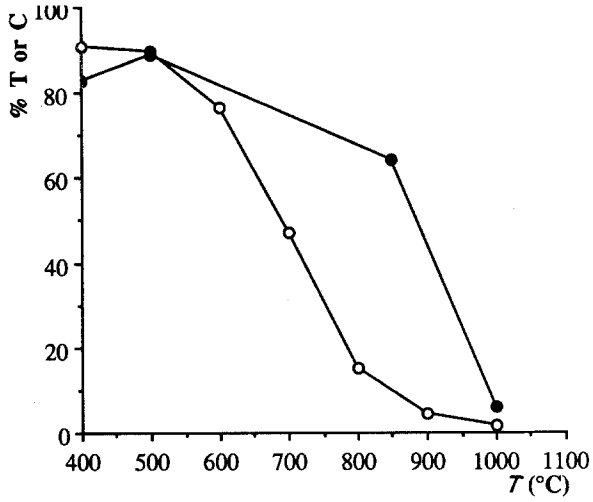

Figure 6 Relative proportion of tetragonal (or cubic) phase as a function of calcination temperature, for the series (○) Z_1 and (●) Z_2.

by using the refined scale factors from the Rietveld method as discussed in [10]. Owing to the highly defective nature of the sample, the refinements are not perfect. However, the quantitative analysis is not very sensitive to small misfits in the observed versus calculated patterns. Fig. 7 shows, as an example, the observed and calculated patterns for the sample Z_1 (800).

For the two precursors the phase transformation sequence was the same, i.e. ZrO_2 (amorphous) → ZrO_2 (tetragonal or cubic) → ZrO_2 (tetragonal + monoclinic) → ZrO_2 (monoclinic). Nevertheless, the transformation from tetragonal (T) to monoclinic (M) structure took place at higher temperatures for the Z_2 series than for the Z_1 one, as shown in Fig. 6.

For Z_1 (400) and Z_2 (400), a better fit between experimental and calculated spectra was obtained by the Rietveld method assuming a cubic (C) structure, compared to the tetragonal one. We attempted to verify this result by applying the peak profile refinement method to the 400 reflection, as done by Benedetti *et al.* [11]. This analysis was not conclusive in the present case, due to the weak intensity of the 400 peak with respect to the background.

The apparent and effective crystallite sizes, as determined from XRD, from the $1\,1\,\bar{1}$ (M) and $1\,0\,1$ (T) reflections, are compared with results obtained by other techniques in Table II. In some samples the contributions of size and strain to line broadening could not be separated, so that the distinction between effective and apparent crystallite sizes was no longer possible. Microstrain values are shown in Table III. These values appear to be quite high for the samples calcined at low temperatures (up to 600 °C) but they decrease steadily with increasing temperature.

4. Discussion

Both series of powders exhibited a rather similar morphological evolution after crystallization. As the calcination temperature increased, crystallite growth occurred first and crystal boundaries were then

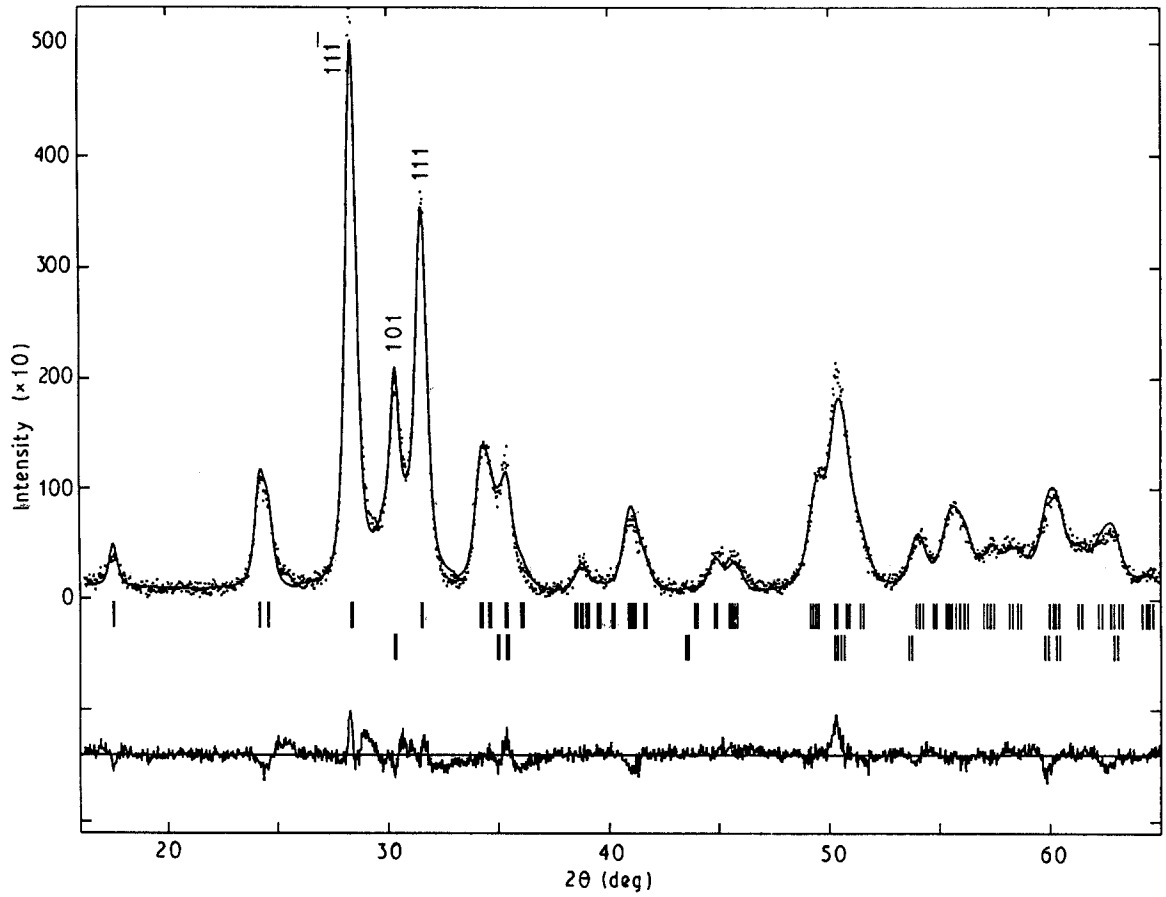

Figure 7 Observed (points) and calculated (line) patterns by the Rietvels method for sample Z_1 (800). The reflection markers ($k_{\alpha 1,\alpha 2}$ doublet) indicate the positions of the Bragg reflections of the monoclinic (top) and tetragonal (bottom) phases. Some important reflections have been labelled.

TABLE II Crystallite and particle sizes depending on calcination temperature, T

Series	T(°C)	d(nm)[a]		d_x(nm)[b]		D(nm)[c]
		CTEM	HREM	M structure	T structure	BET
Z_1	400		4–6	4 (3)	5 (3)	9
	500	6–14		8 (5)	8 (6)	16
	600	9–25		17 (9)	11 (9)	41
	700	12–30	< 13	16 (11)	11 (11)	74
	800		< 20	16(13)	(9)	134
	900			22(16)	(7)	164
	1000			30(21)	(4)	192
Z_2	400		4– 6	(4)	(4)	14
	500		8–17	(10)	(10)	16
	850		12–17	13 (12)	18 (15)	86
	1000			25(20)	(3)	257

[a] Crystallite size (min–max) determined by CTEM and HREM.
[b] Effective crystallite size determined by XRD, apparent size being given in parentheses.
[c] Equivalent diameter determined by BET.

TABLE III Microstrains, ε determined by XRD

Series	T(°C)	ε (× 10^{-2})		
		$(1\,1\,\bar{1})_M$	$(1\,1\,1)_M$	$(1\,0\,1)_T$
Z_1	400	2.7		2.0
	500	1.7	1.5	1.2
	600	1.0	0.9	1.2
	700	0.6	0.6	0.1
	800	0.5	0.7	
	900	0.4	0.5	
	1000	0.3	0.4	
Z_2	850	0.29	0.62	0.32
	1000	0.29	0.30	

formed by sintering. This evolution is consistent with the decrease in specific surface area measured by BET.

In the samples calcined at the lowest temperatures, quite high values of microstrain were determined. They are likely induced by both a high density of structural defects (the crystallization not being completed) and the presence of impurities (like sodium in Z_1 and chlorine in Z_2), which are eliminated at higher temperatures. Benedetti *et al.* [11] reported lower microstrain values ($\varepsilon < 0.003$) for samples calcined at 400 °C, but after 24 h calcination. Other authors [12, 13] reported values of the same order of magnitude as determined here.

A good agreement (Table II) was found between crystallite size values determined by TEM as well as HREM and those obtained by XRD, for the Z_1 samples calcined at temperatures between 400 and 700 °C, and for the Z_2 samples calcined between 400 and 850 °C. In the samples calcined at higher temperatures the complex contrast of the TEM images made the determination of the crystallite size almost impossible. Taken altogether, these results show a regular increase in the crystallite size at increasing temperature for both T and M phases, up to 700 °C for Z_1

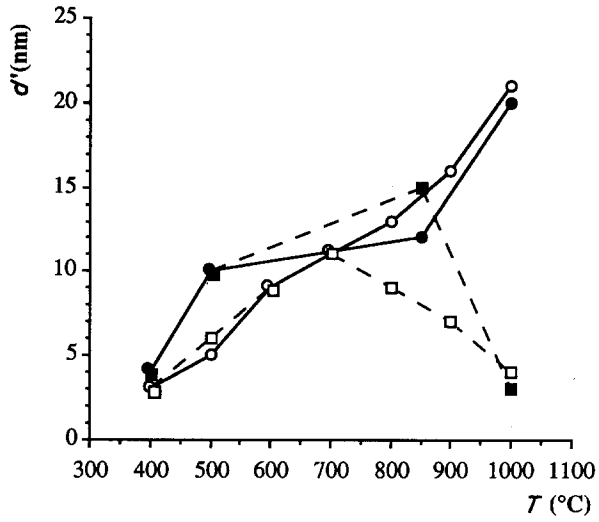

Figure 8 Influence of the calcination temperature on the apparent crystallite size, d', for the tetragonal phase in the series (□) Z_1 and (■) Z_2 and for the monoclinic phase in the series (○) Z_1 and (●) Z_2.

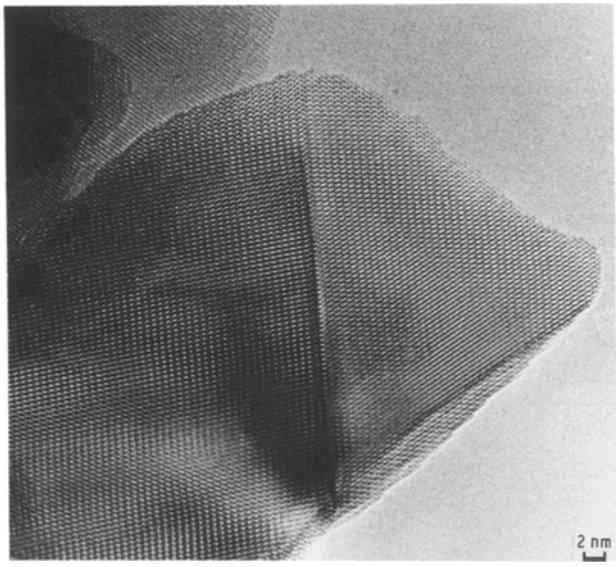

Figure 9 HREM image of sample Z_2 (1000) showing a monoclinic twined particle.

and up to 850 °C for Z_2 (Fig. 8). At higher temperatures, as the phase transformation proceeds, the crystallite size of the M phase, d_M, increases steadily whereas that of the T phase, d_T, diminishes. Such a decrease of d_T seems to be explained by a partial transformation inside the crystallites [9]. For the Z_1 series, d_T never exceeds 11 nm, being always equal to or smaller than d_M. Inversely, d_T for the Z_2 series increases up to 18 nm, being equal to or larger than d_M for $T < 850$ °C. The smaller crystallite size for the M phase is likely to be explained by a twinning mechanism for the phase transformation, so that one tetragonal crystallite gives rise to two monoclinic ones, as suggested by Murase *et al.* [2]: this mechanism was effectively observed in the samples of this series (Fig. 9).

The crystallite growth at increasing calcination temperature appears to be slower for Z_1 than for Z_2. For instance, the crystallite sizes for both phases in Z_2 (500) are almost twice those in Z_1 (500) (we could compare only apparent sizes in this case). Consequently, the larger crystallite size for the T phase in Z_2 (850), compared with that of Z_1 (800) in which the transformation T → M is more advanced, appears to indicate that the stability of the T phase is not determined by a size factor. The stabilization of the tetragonal phase in the Z_2 series could be related to the impurity content, especially chlorine, in these powders, the chlorine content being 1.6 wt % in Z_2 (400) and 0.2 wt % in Z_2 (850)). In fact, another marked difference between Z_1 and Z_2 was the presence of a large amount of superficial pores in the powders prepared from the Z_2 precursor and such a porosity can also be induced by chlorine inclusions.

5. Conclusion

The sequence of phase transformations occurring in both series of powders was the same, i.e. A → C or T → M. Nevertheless, important morphological and structural differences were found between the two series depending on the precursor, which can be revealed only by high-resolution structural studies.

It is not possible to determine unambiguously whether the present powders crystallize first in the cubic or in the tetragonal structure, but in view of the high microstrain values (due to the high concentration of defects) and of the very small difference between the two structures, such a discrimination is irrelevant from a crystallographic point of view.

XRD and TEM studies show that the crystallite size is not the prominent factor determining the stability of the tetragonal phase at low temperature but the presence of impurities such as sodium and chlorine seems to play the main role.

Acknowledgement

We thank Mr D. Urffer, Société Européenne des Produits Réfractaires, who provided the samples, for stimulating discussions on the subject.

References

1. F. WU and S. YU, *J. Mater. Sci.* **25** (1990) 970.
2. Y. MURASE and E. KATO, *J. Amer. Ceram. Soc.* **66** (3) (1983) 196.
3. M. G. BLANCHIN, L. A. BURSILL and E. BERNSTEIN, *Ind. Céram.* **835** (1989) 114.
4. H. M. RIETVELD, *Acta Crystallogr.* **22** (1967) 151.
5. TH. DE KEIJSER, J. I. LANGFORD, E. J. MITTEMEIJER and A. B. P. VOGELS, *J. Appl. Crystallogr.* **15** (1982) 308.
6. J. I. LANGFORD, *ibid.* **11** (1978) 10.
7. J. I. LANGFORD, D. LOUER, E. J. SONNEVELD and J. W. VISSER, *Powder Diff.* **3** (1986) 211.
8. J. RODRIGUEZ, M. ANNE and J. PANNETIER, Strap I. L. L. Internal Report 87RO14T (1987).
9. E. BERNSTEIN, Doctoral thesis, University of Lyon I (1990).
10. J. RODRIGUEZ and J. FONTCUBERTA, *J. Mater. Sci.* **22** (1987) 1001.
11. A. BENEDETTI, G. FAGHERAZZI, S. ENZO and M. BATTAGLIARIN, *J. Appl. Crystallogr.* **21** (1988) 543.
12. T. MITSUHASHI, M. ICHIARA and V. TATSUKE, *J. Amer. Ceram. Soc.* **57** (1974) 97.
13. T. KOSMAC, R. GOPALAKRISHNAN, V. KRASEVEC and M. KOMAC, *J. Phys.* **47** (1986) C1-43.

Received 15 October 1991
and accepted 17 February 1992